Journal of Applied Physics

$CdCl_2$ passivation of polycrystalline CdMgTe and CdZnTe absorbers for tandem photovoltaic cells

Cite as: J. Appl. Phys. **123**, 203101 (2018); https://doi.org/10.1063/1.5023811
Submitted: 28 January 2018 . Accepted: 24 April 2018 . Published Online: 22 May 2018

Drew E. Swanson, Carey Reich, Ali Abbas, Tushar Shimpi, Hanxiao Liu, Fernando A. Ponce, John M. Walls, Yong-Hang Zhang, Wyatt K. Metzger, W. S. Sampath, and Zachary C. Holman

$CdCl_2$ passivation of polycrystalline CdMgTe and CdZnTe absorbers for tandem photovoltaic cells

Drew E. Swanson,[1,2] Carey Reich,[3] Ali Abbas,[4] Tushar Shimpi,[3] Hanxiao Liu,[5] Fernando A. Ponce,[5] John M. Walls,[4] Yong-Hang Zhang,[1] Wyatt K. Metzger,[2] W. S. Sampath,[3] and Zachary C. Holman[1]

[1]*School of Electrical, Computer, and Energy Engineering, Arizona State University, Tempe, Arizona 85287, USA*
[2]*National Renewable Energy Laboratory, Golden, Colorado 80401, USA*
[3]*Mechanical Engineering Department, Colorado State University, Fort Collins, Colorado 80523, USA*
[4]*Loughborough University, Loughborough, United Kingdom*
[5]*Department of Physics, Arizona State University, Tempe, Arizona 85287, USA*

(Received 28 January 2018; accepted 24 April 2018; published online 22 May 2018)

As single-junction silicon solar cells approach their theoretical limits, tandems provide the primary path to higher efficiencies. CdTe alloys can be tuned with magnesium (CdMgTe) or zinc (CdZnTe) for ideal tandem pairing with silicon. A II-VI/Si tandem holds the greatest promise for inexpensive, high-efficiency top cells that can be quickly deployed in the market using existing polycrystalline CdTe manufacturing lines combined with mature silicon production lines. Currently, all high efficiency polycrystalline CdTe cells require a chloride-based passivation process to passivate grain boundaries and bulk defects. This research examines the rich chemistry and physics that has historically limited performance when extending Cl treatments to polycrystalline 1.7-eV CdMgTe and CdZnTe absorbers. A combination of transmittance, quantum efficiency, photoluminescence, transmission electron microscopy, and energy-dispersive X-ray spectroscopy clearly reveals that during passivation, Mg segregates and out-diffuses, initially at the grain boundaries but eventually throughout the bulk. CdZnTe exhibits similar Zn segregation behavior; however, the onset and progression is localized to the back of the device. After passivation, CdMgTe and CdZnTe can render a layer that is reduced to predominantly CdTe electro-optical behavior. Contact instabilities caused by inter-diffusion between the layers create additional complications. The results outline critical issues and paths for these materials to be successfully implemented in Si-based tandems and other applications. *Published by AIP Publishing*. https://doi.org/10.1063/1.5023811

I. INTRODUCTION

Silicon currently makes up 90% of the global PV market[1] with a record cell efficiency of 26.7% and a theoretical limit of 29.4%.[2,3] As silicon approaches the proposed single-junction efficiency limit, tandem solar cells provide the primary path to increased efficiencies beyond 30%.[4] By utilizing proven and cost-effective technologies, tandems hold a potential for continued reductions in the levelized cost of energy.[5,6] High-efficiency tandems can be achieved by marrying the two most mature and low-cost flat-plate PV technologies: silicon and CdTe. However, in a two-wire tandem cell paired with silicon (1.12 eV bandgap), detailed-balance and spectral efficiency predict that the top cell will provide optimum performance with an absorber bandgap of approximately 1.7 eV.[7,8] Presently no photovoltaic material has this bandgap, is inexpensive, and has demonstrated reliability.

CdTe, however, has a bandgap that is only slightly too small (1.5 eV) for optimal pairing with silicon. Polycrystalline CdTe has shown significant advancement in performance in the last 5 years moving from 16 to 22% record cell efficiency.[2,9] It is currently one of the largest US manufactured solar cell technologies and a direct competitor with silicon and fossil fuel technologies.[1] By alloying with magnesium (CdMgTe) or zinc (CdZnTe), the bandgap can be increased from 1.5 eV for CdTe to the modeled 1.7 eV ideal top-cell band gap.[10,11] CdTe alloys have played a large role in the recent advancement of CdTe by passivating the bulk and interfaces of CdTe absorbers.[12,13] Thus far, polycrystalline II-VI (MgZnCd)(SeTe) materials are relatively unexplored as the primary absorber but hold the greatest promise for inexpensive, high-efficiency top cells that can be quickly deployed in the market using existing polycrystalline CdTe manufacturing lines combined with mature silicon production lines.

Single-crystal CdMgTe and CdZnTe absorbers have demonstrated capability with verified efficiencies of 15.3% and 16.4% at ~1.7 eV bandgaps;[14,15] however, record efficiencies for polycrystalline CdMgTe and CdZnTe absorbers are currently both below 7%.[16–19] In both cases, the authors report absorber degradation during passivation treatments resulting in a defect-dense absorber. Annealing treatments have been reported for improved material quality; however, without a chlorine vapor present, cell efficiency remains below 1%.[19] A key difference between single-crystal and polycrystalline II-VI cells has been the need for a chlorine-based passivation treatment to remove defects induced during growth. $CdCl_2$ has been reported to have various effects on CdTe including recrystallization, grain growth, stacking fault removal, and grain boundary passivation by putting chlorine on tellurium vacancies.[20–23] However, initial attempts at $CdCl_2$ passivation of CdMgTe and CdZnTe have revealed reductions in the

bandgap of both absorbers during $CdCl_2$ passivation.[16,18,19] This work aims to study this $CdCl_2$-induced degradation and develop a more comprehensive understanding of the reactions occurring. To this end, we passivate three solar cell sample sets: a 1.7 eV CdMgTe absorber, a 1.7 eV CdZnTe absorber, and a 1.5 eV CdTe reference absorber. $CdCl_2$ treatments are applied for a series of temperatures between 380 and 460 °C. The resulting chemical and physical processes occurring in the absorbers and cells are revealed with transmittance, quantum efficiency (QE), photoluminescence (PL), transmission electron microscopy, energy-dispersive x-ray spectroscopy, and time-resolved photoluminescence (TRPL).

II. MATERIALS AND METHODS

This work explores three different primary absorbers: CdTe, CdMgTe, and CdZnTe absorbers were grown using a novel co-sublimation process developed at Colorado State University. A fully-automated single-vacuum PV manufacturing tool utilizes multiple inline close space sublimation (CSS) sources with automated substrate control. Sources have independent temperature control and multiple vapor pressures can be concurrently developed within each CSS source. This technology allows CdTe to be controllably alloyed with magnesium, zinc, and selenium.[10,13] The single-vacuum deposition system, processing details, and hardware are described in Ref. 24. In the case of CdZnTe, films were deposited in a separate chamber and then transferred to the single-vacuum deposition system for further processing.[10]

Cell structures are depicted in Fig. 1 with approximate thicknesses and doping concentrations as reported in the literature. Traditional CdTe contacts were used: a commercially available Pilkington Tec10 soda-lime glass with a SnO_2:F (FTO) layer followed by a sputtered magnesium zinc oxide (MZO) buffer for the electron contact and an evaporated tellurium layer for the hole contact.[25–27] The contacts had been optimized in the past for a CdTe absorber; here no further re-optimization for the alloy absorbers was performed.

All three sample sets received similar $CdCl_2$ treatments with varying intensity by modifying the temperature of the $CdCl_2$ sources from 380 to 460 °C. The $CdCl_2$ treatment time was maintained at 180 s but was modified to a vapor treatment by bringing the top heater of the $CdCl_2$ source to the same temperature as the bottom source.[24] This resulted in no $CdCl_2$ deposition during treatment, which makes the variation in passivation more controllable. A methanol rinse was performed after treatment to remove any potential residue. The cells did not receive any post-fabrication anneal or intentional copper doping treatment.

To reduce degradation during passivation, a CdTe capping layer was deposited on each absorber (Fig. 1). Earlier studies reported that a thin CdTe capping layer reduced the reactive nature of CdMgTe contacts on CdTe absorbers during $CdCl_2$ passivation.[28] It appeared that the CdTe cap prevented the complete loss of magnesium from the CdMgTe contact but did not prevent localized magnesium loss at the grain boundaries.

Samples underwent extensive materials characterization at different fabrication stages.

Absorber transmittance (T) was recorded with a PerkinElmer LAMBDA 950 UV/VIS/NIR spectrophotometer equipped with a 150 mm integrating sphere accessory. Bandgaps were calculated using the Tauc plot method, where $(\alpha h\lambda)^2$ is plotted against photon energy, hv, and the linear portion of $(\alpha h\lambda)^2$ is extrapolated to where $\alpha = 0\,cm^{-1}$ (i.e., the x-axis).[10,29]

Cross-sectional cathodoluminescence (CL) spectroscopy used a scanning electron microscope, with a spectrometer equipped with a 1200 l/mm grating and a GaAs photomultiplier tube. The CL measurements were taken at 298 K, with an electron beam current of 2.0 nA and an acceleration voltage of 9 kV. Monochromatic CL images were obtained by setting the monochromator to a specific wavelength and recording the spatial variations of the light emission intensity.

Samples for transmission electron microscopy (TEM) were prepared by focused ion beam (FIB) milling using a

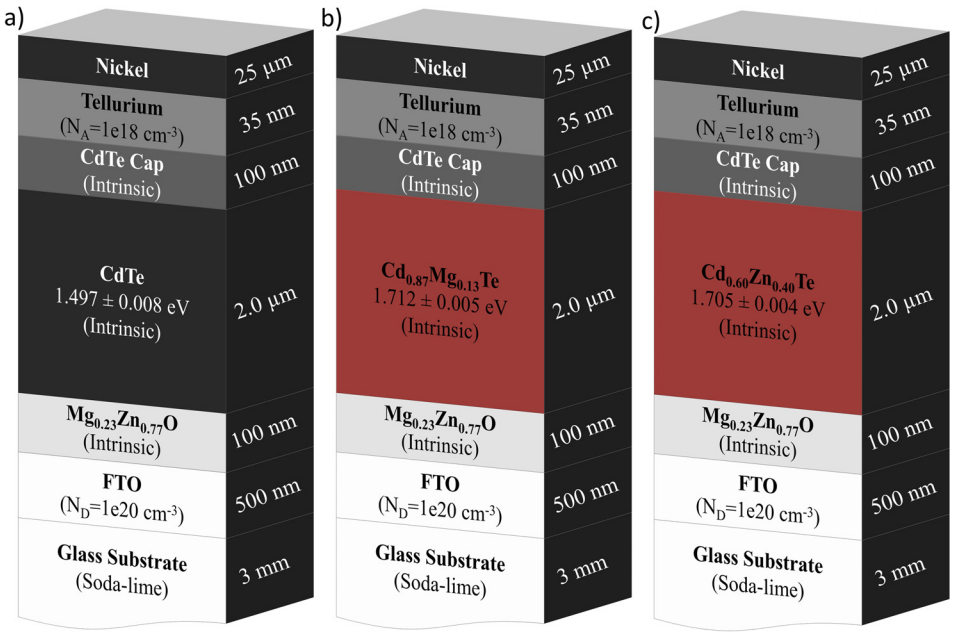

FIG. 1. Cell structure for each of the three absorbers studied: (a) CdTe, (b) CdMgTe, and (c) CdZnTe. Only the absorber layer was purposely varied between cells. Note that the back contact (Te/Ni) is only present for electrical characterization as identified. The average as-deposited bandgaps are identified for all three sample sets.

dual-beam FEI Nova 600 Nanolab. Cross-sectional samples were prepared through the coating into the glass substrate by a standard *in situ* lift-out method. An electron-beam-assisted platinum (e-Pt) over-layer was deposited followed by an ion-assisted layer to define the surface and homogenize the final thinning of the samples down to 100 nm. TEM analysis was performed with a Tecnai F20 operating at 200 kV to investigate the detailed microstructures of the solar cell cross sections.

The TEM system was equipped with an Oxford Instruments X-max N80 TLE SDD energy-dispersive X-ray spectroscopy (EDX) detector and operated in STEM mode to acquire elemental distribution maps and line scans. The maps were collected in a single frame using a long dwell time, as well as a small condenser aperture (70 μm) to minimize drift and beam spread during data collection.

Steady-state photoluminescences (PL) used an excitation wavelength of 520 nm at ~40 suns intensity. A 570-nm long-pass filter was used to minimize any signature of the excitation energy; however, a small tail is present and identified in the shown data. PL was measured from the glass side and estimated to probe the first ~500 nm of the various absorbers. All PL intensities are normalized for comparison across absorbers.

Single-photon time-resolved photoluminescence (TRPL) was performed with a pulsed laser tuned to a wavelength of 640 nm firing at 1 MHz with an average power of 1 mW. Cells were measured from the glass side and the laser predominantly excites carriers within the first 500 nm of the absorber. Data presented are representative of the substrate. A bi-exponential fit is used to describe and compare the results.[30]

External quantum efficiency (QE) was measured on cells with the tellurium and nickel hole contact present; each substrate was finished into 0.6 cm^2 small-area devices with roughly 10 cells for each condition. A representative cell, near average for the data set, is presented.

III. RESULTS AND DISCUSSION

This work explores identical sample sets with three different primary absorbers: CdTe, CdMgTe, and CdZnTe. All three sample sets use traditional CdTe contacts and received similar $CdCl_2$ treatments at temperatures ranging from 380 to 460 °C.

A. Passivation of CdTe

CdTe absorbers are presented to give reference to the $CdCl_2$ intensities required to initiate passivation characteristics and give scale to the onset of degradation in the other absorbers. Figure 2 gives the transmittance (T), quantum efficiency (QE), and photo-luminescence (PL) plots for the CdTe absorber for different $CdCl_2$ passivation temperatures. A 1.5-eV bandgap is marked with a dashed line showing agreement across the various samples. CdTe maintains its composition after passivation, with no significant shift in the band edge of the material with increasing passivation intensity.

An increase in the collection of carriers generated deep within the absorber was observed in QE from 700 to 830 nm

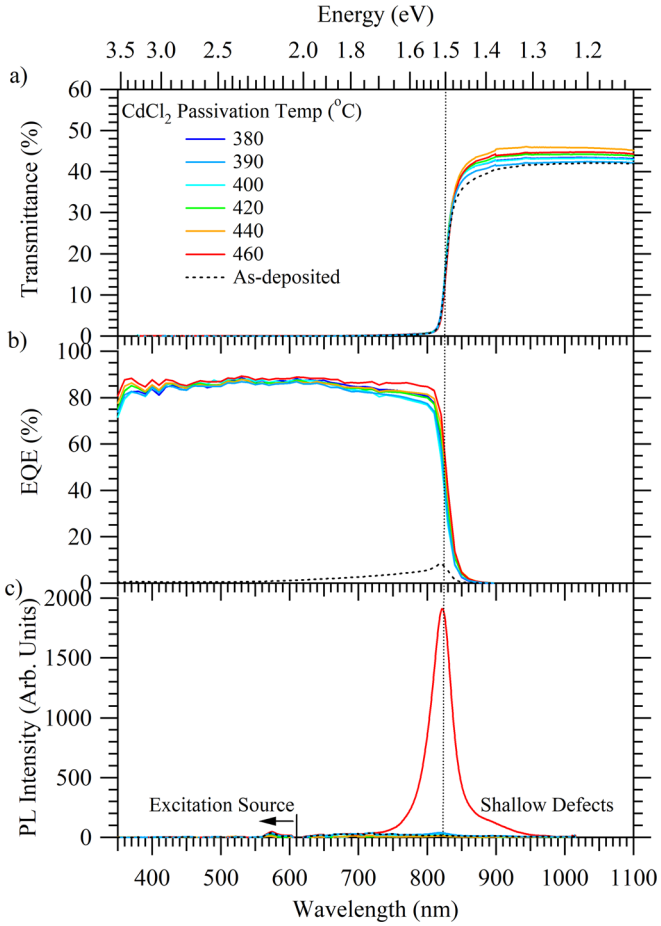

FIG. 2. (a) Transmittance, (b) external quantum efficiency, and (c) photo-luminescence for a CdTe absorber treated with $CdCl_2$ passivation temperatures from 380 to 460 °C. Dashed lines at 1.5 eV are plotted for reference.

with increasing temperature. At the highest temperature studied (460 °C), there are two orders of magnitude increase in PL signal. This indicates the onset of passivation of the CdTe absorber. The passivation treatments are intentionally light compared to the previous work on this manufacturing equipment;[24,31] however, at 460 °C the onset of bulk passivation was observed.

B. Passivation of CdMgTe

Figure 3 shows the T, QE, and PL for the CdMgTe absorber with increasing $CdCl_2$ passivation temperatures. Dashed lines corresponding to 1.7 and 1.5 eV are plotted for reference. Transmittance of the as-deposited CdMgTe cell shows a dominant 1.7-eV band edge with a minor 1.5-eV band edge which appeared after the deposition of the 100-nm CdTe capping layer.

Similar to CdTe, the QE response increases significantly in the samples after 380 °C $CdCl_2$ passivation. With increasing $CdCl_2$ temperature, transmittance (T) data indicate the dominant optical band edge shifts directly from 1.7 to 1.5 eV, which is consistent with a loss in magnesium from the bulk absorber. The QE data present a similar trend as carrier collection is increasing between the 1.5-eV and 1.7-eV absorption band edges with increasing temperature, giving further indication of localized magnesium loss resulting in the formation of CdTe.

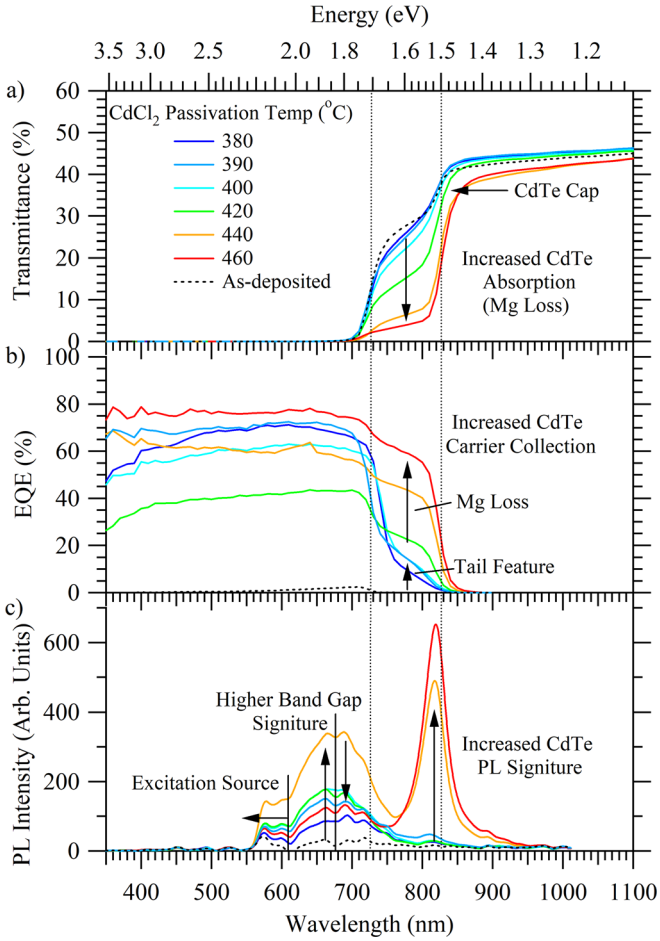

FIG. 3. (a) Transmittance, (b) external quantum efficiency, and (c) photoluminescence for a CdMgTe absorber with $CdCl_2$ passivation temperatures from 380 to 460 °C. Dashed lines at 1.5 and 1.7 eV are plotted for reference.

QE initially presents a tail signature at 380 °C, which increases with $CdCl_2$ temperature. This tail is not present in either of the other absorbers and is not associated with the CdTe capping layer as the previous work showed no correlation between the CdTe capping layer thickness and the tail signature.[18] The tail feature may represent the onset of loss at grain boundaries, a loss reaction seen in CdMgTe hole contact research.[28]

The PL data display an increasing peak at ~1.8 eV with increasing passivation temperature. Note that 1.8 eV is significantly higher than the T and QE band edges, which implies a higher bandgap material forms. This is later attributed to zinc diffusion from the MZO electron contact. The addition of zinc at the front of the device increases the local bandgap, shifting the PL peak from 1.7 to 1.8 eV. This is not observed in T or QE as both measurements detect the lowest prevalent bandgap at 1.7 eV.

Beginning at ~440 °C, an additional PL peak emerges at 1.5 eV; thus, two separate alloys are photo-luminescing at 1.8 and 1.5 eV. Supported by T and QE, this suggests that the magnesium loss is non-uniform, resulting in a compositional spatial inhomogeneity within the absorber. An increased passivation temperature of 460 °C resulted in a further increase in the 1.5 eV peak and a decrease in the 1.8 eV peak, implying continued loss of magnesium from the CdMgTe absorber regions and passivation of the growing CdTe absorber regions.

C. Passivation of CdZnTe

Figure 4 gives the T, QE, and PL for the CdZnTe absorber over increasing $CdCl_2$ passivation temperatures. Here, 1.7- and 1.5-eV dashed lines are plotted for reference. Transmittance of the as-deposited CdZnTe cell shows a dominant 1.7-eV band edge with a minor 1.5-eV band edge, which appeared after the deposition of the 100-nm CdTe capping layer.

Similar to CdTe and CdMgTe, the QE response increases with 380 °C $CdCl_2$ passivation, however, to a lesser degree until significant zinc loss is observed. Transmittance of CdZnTe shows a similar shift from 1.7 to 1.5-eV band edges as CdMgTe; however, the formation of the optically dominant 1.5-eV band edge presents as a gradual downward shift from 1.7 to 1.5 rather than only two distinct peaks of 1.7 and 1.5 eV with varying magnitude, as observed for CdMgTe. The QE data show a similar single band edge shift, suggesting that a single alloy was present during loss, and zinc diffused throughout the bulk absorber to maintain a single alloy. The PL indicates a peak intensity at 1.7 eV for 380–400 °C $CdCl_2$ passivation, in agreement with the band edges presented in T and QE. As the passivation temperature

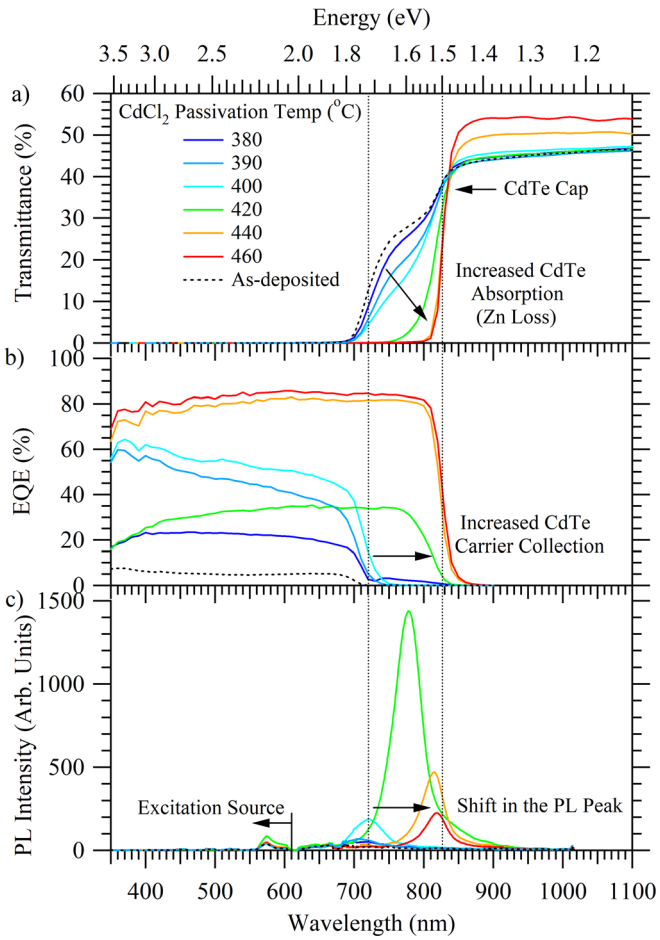

FIG. 4. (a) Transmittance, (b) external quantum efficiency, and (c) photoluminescence for a CdZnTe absorber with $CdCl_2$ passivation temperatures from 380 to 460 °C. Dashed lines at 1.5 and 1.7 eV are plotted for reference.

is increased to 420 °C, the peak begins to shift from 1.7 to 1.5 eV as a single peak with a similar onset to that in the QE spectra. At 440 °C, the peak begins to saturate at 1.5 eV, suggesting that an optically dominant amount of the CdZnTe absorber has been converted to CdTe, in agreement with T and QE. By 460 °C, an optically dominant 1.5-eV band edge is present in both alloys; however, the CdZnTe shift appears to onset at lower temperatures than the CdMgTe.

D. Identifying loss location

CdMgTe and CdZnTe absorbers show a reduction in bandgap with increasing $CdCl_2$ passivation temperatures associated with the loss of the magnesium and zinc. The loss mechanisms are distinct for each alloy, and thus STEM and EDX were performed to identify where the loss was occurring and give further insight into the loss reaction for each alloy.

Figure 7 shows a cross-section STEM/EDX image of the CdMgTe absorber: as-deposited, and after a 390 °C, 420 °C, or 440 °C $CdCl_2$ passivation. The MZO electron contact appears to have reacted with the CdMgTe layer as significant zinc and magnesium have diffused between the layers. It appears to occur upon deposition of CdMgTe and increase in severity with increasing passivation temperature. Inter-diffusion of zinc and magnesium at the front of the device could potentially increase its local bandgap, providing a possible explanation for the increased 1.8-eV PL emission observed in Fig. 3.

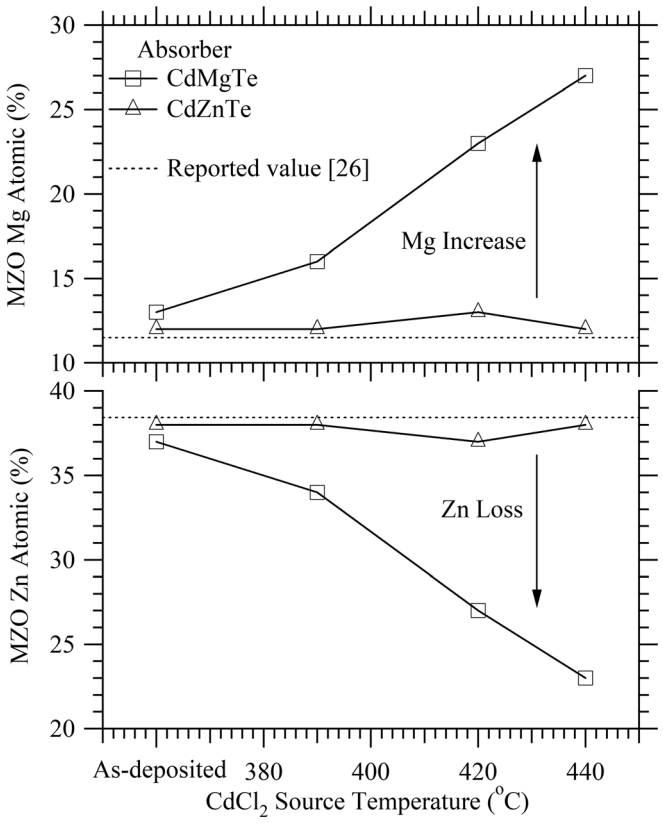

FIG. 5. Average atomic percentatges of magnesium and zinc in the MZO buffer layer, as measured by EDX line scans of the TEM images presented in Figs. 7 and 9.

Figure 5 gives the atomic percentages of magnesium and zinc in the MZO over the various treatments. With increasing passivation, the MZO composition shifts significantly. The electron affinity of the MZO layer is dependent on its stoichiometry;[26] thus any change in the zinc and magnesium concentration will change the band alignment at the MZO/CdMgTe interface. This MZO degradation will need to be addressed if it is to be used as a suitable electron contact for CdMgTe.

The as-deposited CdMgTe absorber shows magnesium non-uniformity throughout the bulk with a standard deviation of ∼1.5 at. % or ∼0.023 eV in the Fig. 7 EDX map. The magnesium loss appears to occur in two stages: early onset at the grain boundaries, and then bulk loss initiating at the front and progressing towards the rear. At 380 °C, EDX line scans in Fig. 6 show a sudden drop in magnesium signal along the grain boundaries. TEM images in Fig. 7 show small voids forming along the grain boundaries, consistent with localized degradation. The magnesium loss increases at the grain boundaries with preferential loss towards the front of the device as the passivation temperature increases to 420 °C, while at the same time voids multiply and increase in size along the grain boundaries. The magnesium loss at the grain boundary is consistent with the growth of the tail feature shown in the QE of Fig. 3.

At 390 °C, chlorine and oxygen signatures are present at the grain boundaries. A chlorine signature along the grain boundaries is typical for CdTe passivation,[20] but the strong corresponding oxygen signal is atypical. At 420 °C, no significant change in the chlorine signature was observed, but large voids begin to form near select grain boundaries with corresponding oxygen signals. The oxygen presence in combination with growing voids appears to be a magnesium loss reaction signature, as magnesium is favorable to oxidize and may drive this reaction.[10,28]

Magnesium bulk loss is prevalent at 440 °C passivation, with voids throughout the absorber and corresponding strong chlorine, oxygen, and magnesium signals. Bulk magnesium loss was preferential towards the front of the device and

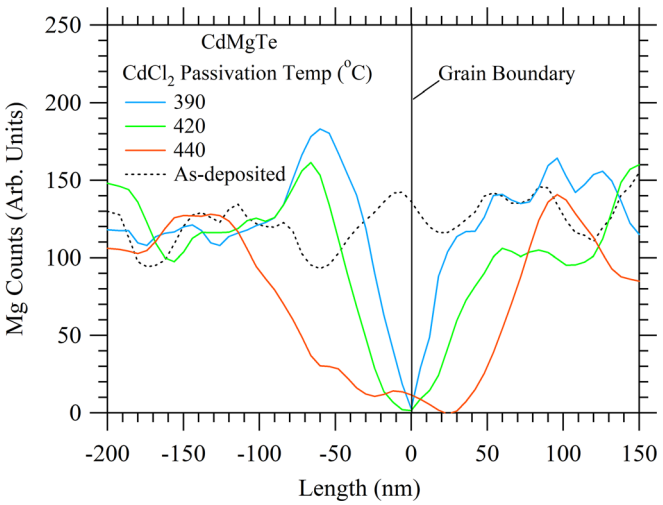

FIG. 6. A line-scan of the magnesium EDX image of the as-deposited sample, and after 390, 420, and 440 °C $CdCl_2$ passivation presented in Fig. 7.

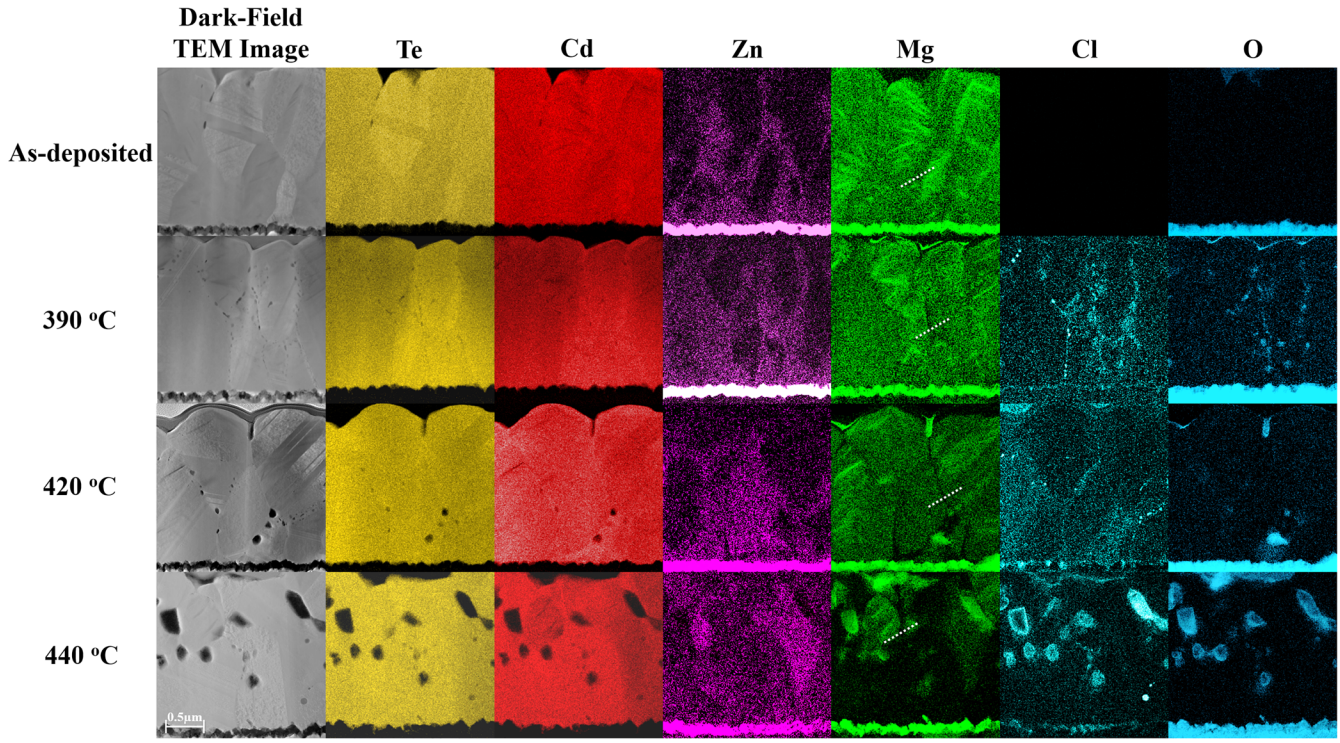

FIG. 7. Cross-section TEM and EDX of CdMgTe: As-deposited, and after 390, 420, and 440 °C $CdCl_2$ passivation. Figure 6 line scan locations are identified.

progressed toward the hole contact with voids acting as potential sinks for magnesium. This supports the compositional segregation hypothesized in response to the T, QE, and PL of Fig. 3.

In CdTe chloride passivation, it has been theorized that chlorine travels down the grain boundaries in an elemental state and preferentially accumulates there.[20,32] The chlorine can remove stacking faults from within the CdTe grains and may passivate the grain boundaries by filling tellurium vacancies, effectively making the grain boundaries less p-type.[23] This can affect both transport and recombination.[33–35] In this research, CdMgTe grain boundaries are proposed to be converted to CdTe when passivated with $CdCl_2$. The combination of localized magnesium loss and chlorine may have significant effects on recombination and transport near grain boundaries. In particular, CdTe compositions can allow for minority carriers to preferentially flow to the lower energy state at the CdTe grain boundary and adjacent regions, thereby increasing dark current and limiting the potential voltage of the cell.[36]

Cross-section cathodoluminescence images of as-deposited and 440 °C $CdCl_2$ passivation CdMgTe absorbers are presented in Fig. 8. The red response corresponds to a ~1.77 eV emission and blue to ~1.5 eV. The as-deposited sample shows a strong 1.77-eV red response throughout the bulk absorber with a faint 1.5-eV blue response at the back from the CdTe capping layer. After the 440 °C passivation treatment, the front 1 μm of the device shifts to a 1.5-eV blue response. This supports the STEM/EDX evidence that the bulk loss initiates at the front of the CdMgTe absorber and progresses towards the rear with increasing passivation intensity.

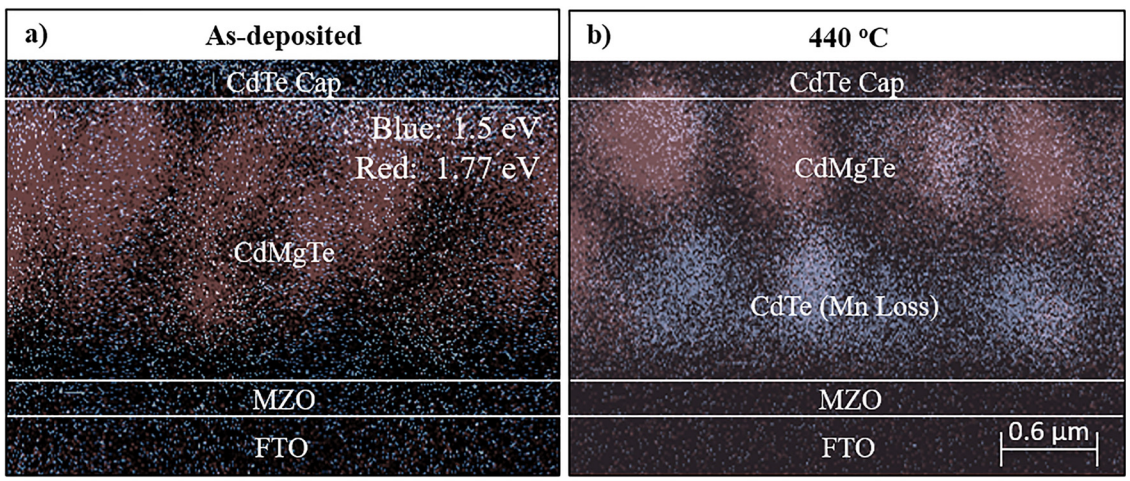

FIG. 8. Cathodoluminescence of the CdMgTe absorber (a) As-deposited and (b) after a 440 °C $CdCl_2$ treatment.

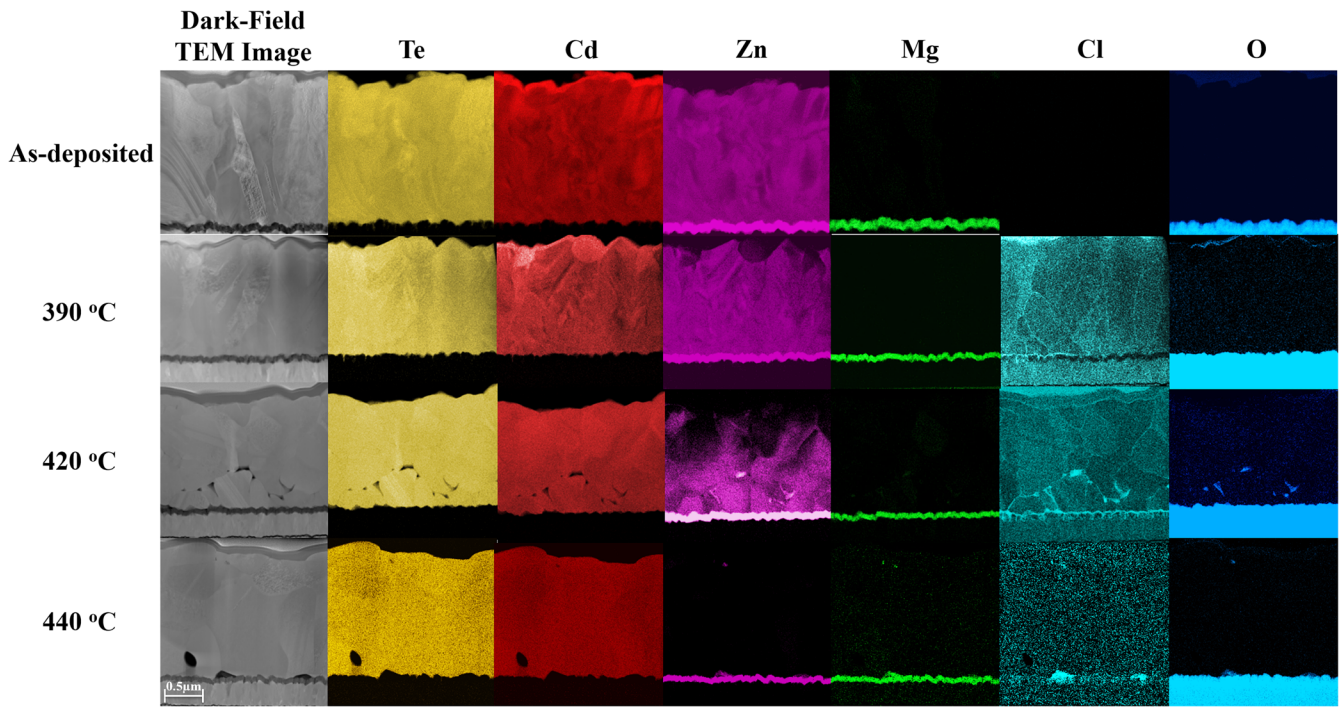

FIG. 9. Cross-section TEM and EDX of CdZnTe: As-deposited, and after 390, 420, and 440 °C $CdCl_2$ passivation.

Figure 9 shows cross-sectional STEM/EDX images of the CdZnTe absorber: as-deposited, and after a 390 °C, 420 °C, or 440 °C $CdCl_2$ passivation. As measured by EDX and PL, there appears to be no diffusion of magnesium or zinc between the CdZnTe absorber and MZO layer. Figure 5 supports this as there was no substantial change in the MZO composition measured in EDX. In addition, there is no corresponding increase in PL emission energy from the targeted 1.7-eV bandgap. This implies that the MZO layer is significantly more stable with CdZnTe than with CdMgTe. Note that with the increased bandgap and reduced electron affinity of the CdZnTe, the MZO/CdZnTe interface will likely require the MZO composition to be changed to achieve similar band offsets as compared to CdTe.[26]

The as-deposited CdZnTe absorber showed zinc nonuniformity throughout the bulk with a standard deviation of ~3.5 at. %. This translates to a bandgap variation of ~0.017 eV, and the zinc EDX map is shown in Fig. 9. At 390 °C, chlorine decorates the grain boundaries with no significant oxygen signature from within the bulk, similar to what is typically seen in $CdCl_2$ passivation of CdTe. At 420 °C, zinc loss initiates from the back of the device with a corresponding reduced concentration of zinc (from x = 0.4 to 0.2) at the front, as observed in PL. Several loss reactions have been proposed in the literature to explain this behavior.[6] Figure 4 shows that a single PL peak is maintained during loss despite the lower bandgap signature observed in T and QE. The zinc is believed to be diffusing at the front, to form a more homogeneous lower-bandgap alloy, while a growing CdTe layer develops at the back and progresses forward. PL was performed using a 520-nm excitation light that has an approximate excitation depth of 400 nm; thus, the developed CdTe layer was likely not probed.

Localized voids form between the CdZnTe at the front and the growing CdTe film at the back. It has been noticed that films passivated around 420 °C are prone to absorber delamination. The recrystallization of CdTe at the back of the device during zinc loss may induce localized stress between the reacted CdTe and CdZnTe absorber, making the films prone to delamination. These voids appear to have a corresponding oxygen and chlorine signal similar to CdMgTe, but with reduced spatial density. By 440 °C, the chlorine signature is significantly reduced at the grain boundaries. Chlorine loss mechanisms have been reported in the CdTe literature at elevated temperatures.[20]

Cross-sectional cathodoluminescence images of as-deposited and 420 °C $CdCl_2$ passivation CdZnTe absorbers are presented in Fig. 10. The red response corresponds to a 1.74-eV emission, green to 1.61 eV, and blue to 1.51 eV. The as-deposited sample shows a strong 1.74-eV red response throughout the bulk absorber with a faint 1.5-eV blue response at the back associated with the CdTe capping layer. After the 420 °C passivation treatment, the back 1 μm of the device shifts to a 1.5-eV blue response. This supports the STEM/EDX evidence that the bulk loss initiates at the back of the CdZnTe absorber and progresses towards the front with increasing passivation intensity. The signature at the front shifts from 1.74 to 1.61 eV in agreement with PL and supporting zinc diffusion at the front to compensate for loss at the back.

E. Time-resolved photoluminescence

Single-photon time-resolved photoluminescence was performed on all three absorber alloys. These curves were fitted with a bi-exponential fit, and the resulting average values (±standard deviation) for the fitted constants Tau_1 and Tau_2 are plotted in Fig. 11.[30] The instrument response function (IRF) represents the inherent equipment delay and thus represents the minimum value that can be measured.

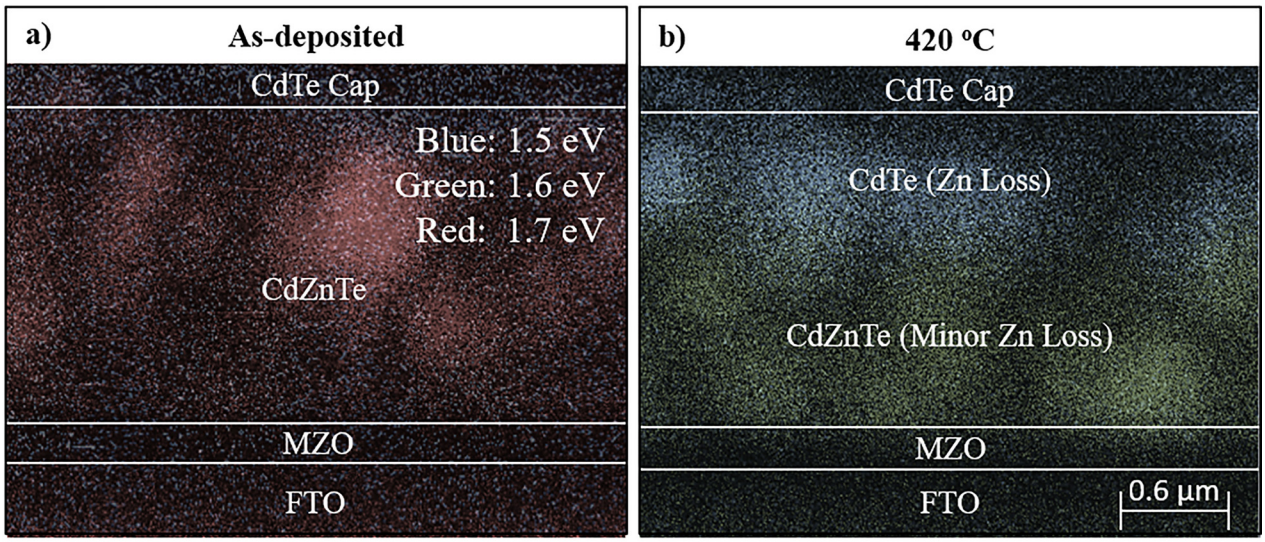

FIG. 10. Cathodoluminescence of the CdZnTe absorber (a) As-deposited and (b) after a 420 °C $CdCl_2$ treatment.

Both lifetime fit constants are low for the CdTe absorbers from 380 to 420 °C, which is associated with the intentional under-passivation of the absorber.[30] At 440 °C, both constants begin to improve and by 460 °C are approaching reported non-selenium passivated CdTe lifetimes of $Tau_2 = 2$–6 ns. Improved QE and PL signatures in Fig. 2 correspond with the increasing lifetime fit constants for the CdTe absorber.

We have shown that the CdMgTe and CdZnTe absorbers undergo significant degradation during passivation, making lifetime approximation convoluted by the potential presence of multiple compositions. Variation in lifetime at the grain boundaries and grain interiors could not be distinguished. CdMgTe and CdZnTe absorbers exhibit low Tau_1 and Tau_2 values until bulk degradation is apparent. Significant improvement in lifetime above 1 ns for Tau_2 is seen but not until after significant zinc loss occurs. This increase in lifetime is associated with the increasing carrier localization into the higher lifetime CdTe material, which is also increasing in volume. With increasing zinc and magnesium loss, the minority carrier lifetimes converge to values similar to CdTe. CdTe lifetimes appear to be similar either as deposited or after CdMgTe and CdZnTe are degraded to CdTe. This implies that magnesium and zinc may be added and removed without irreversibly changing the CdTe absorber.

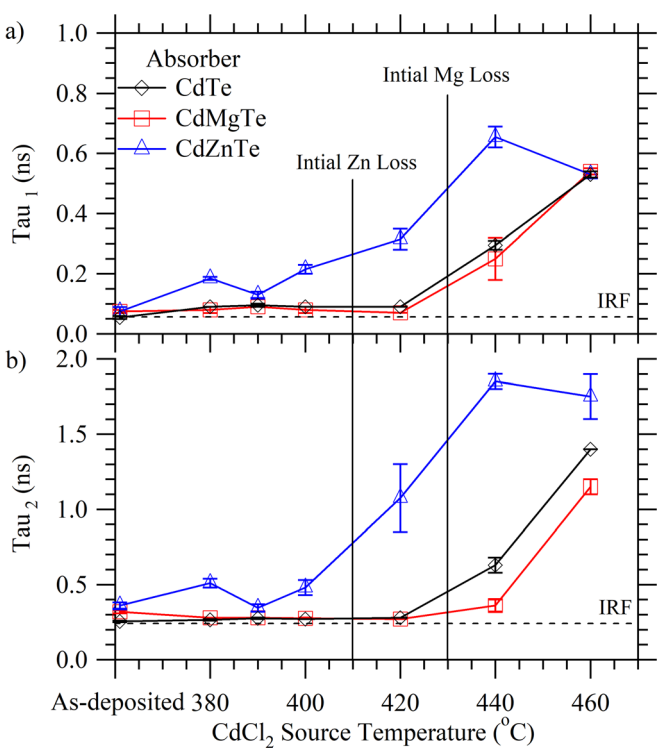

FIG. 11. (a) Tau_1 and (b) Tau_2 bi-exponential fit parameters of single-photon time-resolved photoluminescence of the CdTe, CdMgTe, and CdZnTe absorbers with $CdCl_2$ passivation treatments from 380 to 460 °C.

All three absorbers appear under-passivated from 380 to 400 °C. As expected, a more aggressive $CdCl_2$ passivation treatment to CdTe (460 °C) showed increased PL signature and higher minority carrier lifetimes. As increasing intensities of $CdCl_2$ passivation for CdMgTe and CdZnTe absorbers resulted in alloy degradation, the improved lifetime is primarily associated with the increasing carrier localization into the higher-lifetime CdTe material that is formed. More aggressive passivation treatments are desired; however, methods to mitigate loss must be developed.

IV. CONCLUSION

At the modeled ideal bandgap of 1.7 eV, CdZnTe and CdMgTe absorbers have been deposited using scalable manufacturing processes. Single-crystal CdMgTe and CdZnTe cells have reported efficiencies over 15%, and no fundamental limitation has been yet identified. The largest hurdle to transferring single-crystal performance to polycrystalline materials in II-VI solar cells is currently the need for a $CdCl_2$ passivation step. As-deposited CdMgTe and CdZnTe absorbers exhibited poor performance and low carrier lifetime, indicating a need, similar to CdTe, for $CdCl_2$ passivation. Upon $CdCl_2$ passivation treatments of CdMgTe and CdZnTe absorbers, QE and PL performance improved but were accompanied

by significant degradation. The degradation magnitude and presentation were different for each II-VI alloy.

CdMgTe exhibited inter-diffusion with the MZO electron contact resulting in localized bandgap grading and MZO bulk loss. The magnesium loss appears to occur in two stages: early onset at the grain boundaries, then bulk loss initiating at the front and progressing towards the rear. Localized magnesium loss at the grain boundary is correlated to a tail feature in QE. This loss could theoretically limit the potential voltage of the cell by reducing the maximum possible quasi-Fermi-level splitting and hence undermine the objective of a high-bandgap top cell. This localized magnesium loss will have to be addressed if CdMgTe is to be a suitable top cell.

CdZnTe did not exhibit instability with MZO and thus MZO is identified as a potential electron contact for CdZnTe. MZO will likely require a compositional tuning due to the change in the electron affinity of the CdZnTe as compared to CdTe, for ideal performance. The loss of zinc occurs as a gradual shift from 1.7 to 1.5 eV in T, QE, and PL. Zinc was lost from the back of the device as the formation of CdTe propagated towards the electron contact, as shown in EDX. Unlike CdMgTe, CdZnTe did not present early onset loss at the grain boundaries and had improved minority carrier lifetime compared to CdMgTe degradation at the highest temperatures. Alternative back contacts may be developed to reduce zinc diffusion and permit more aggressive passivation treatments.

Both CdMgTe and CdZnTe appear to undergo degradation and loss of Zn/Mg before passivation treatments are completed. More aggressive passivation treatments are desired; however, methods to mitigate loss must be developed. Passivation treatments containing $MgCl_2$, $ZnCl_2$, magnesium, or zinc vapor pressures may saturate possible loss reactions and reduce alloy degradation. Preliminary work with increased time at lower $CdCl_2$ passivation treatment temperatures shows similar degradation signatures in T and QE, but a comprehensive study has not been performed.

ACKNOWLEDGMENTS

The authors are thankful for funding support from the DOE PVRD DE-EE0007552 and collaborations with Colorado State University, Loughborough University, and the National Renewable Energy Laboratory. The authors are grateful for assistance with the research from Kevan Cameron, Amit Munshi, Andrew Moore, Jason Kephart, Kurt Barth, Marina D'Ambrosio, Christina Moffett, Arthur Onno, and Lauren Swanson.

[1]T. D. Lee and A. U. Ebong, "A review of thin film solar cell technologies and challenges," Renewable Sustainable Energy Rev. **70**, 1286 (2017).
[2]M. A. Green, Y. Hishikawa, W. Warta, E. D. Dunlop, D. H. Levi, J. Hohl-Ebinger, and A. W. Ho-Baillie, "Solar cell efficiency tables (version 50)," Prog. Photovoltaics **25**, 668 (2017).
[3]W. Shockley and H. J. Queisser, "Detailed balance limit of efficiency on p-n junction solar cells," J. Appl. Phys. **32**, 510 (1961).
[4]S. Essig, C. Allebe, T. Remo, J. F. Geisz, M. A. Steiner, K. Horowitz, L. Barraud, J. S. Ward, M. Schnabel, A. Descoeudres, D. L. Young, M. Woodhouse, M. Despeisse, C. Ballif, and A. Tamboli, "Raising the one-sun conversion efficiency of III-V/Si solar cells to 32.8% for two junctions and 35.9% for three junctions," Nat. Energy **2**, 17144 (2017).
[5]A. C. Tamboli, D. C. Bobela, A. Kanevce, T. Remo, K. Alberi, and M. Woodhouse, "Low-cost CdTe/silicon tandem solar cells," IEEE J. Photovoltaics **7**, 1767 (2017).
[6]I. M. Peters, S. Sofia, J. Mailoa, and T. Buonassisi, "Techno-economic analysis of tandem photovoltaic systems," RSC Adv. **6**, 66911 (2016).
[7]J. P. Mailoa, M. Lee, I. M. Peters, T. Buonassissi, A. Panchula, and D. N. Weiss, "Energy-yield prediction for II-VI based thin-film tandem solar cells," Energy Environ. Sci. **9**, 2644 (2016).
[8]Z. Yu, M. Leilaeioun, and Z. Holman, "Selecting tandem partners for silicon solar cells," Nature Energy **1**, 16137 (2016).
[9]NREL, see https://www.nrel.gov/pv/assets/images/efficiency-chart.png for Best Research-Cell Efficiencies (NREL, 2017).
[10]P. S. Kobyakov, A. Moore, J. M. Raguse, D. E. Swanson, and W. S. Walajabad, "Deposition and characterization of CdMgTe thin films grown by a novel cosublimation method," J. Vac. Sci. Technol. A **32**, 021511 (2014).
[11]A. Rohatgi, R. Sudharsanan, S. A. Ringel, and M. H. Macdougal, "Growth and process optimization of CdTe and CdZnTe polycrystalline films for high efficiency solar cells," Sol. Cells **30**, 109 (1991).
[12]Y. Zhao, M. Boccard, S. Liu, J. Becker, X.-H. Zhao, C. M. Campbell, E. Suarez, M. B. Lassise, Z. Holman, and Y.-H. Zhang, "Monocrystalline CdTe solar cell with open-circuit voltage over 1V and efficiency of 17%," Nat. Energy **1**, 16067 (2016).
[13]D. E. Swanson, J. R. Sites, and W. S. Sampath, "Co-sublimation of CdSeTe layers for CdTe solar cells," Sol. Energy Mater. Sol. Cells **159**, 389 (2017).
[14]C. M. Campbell, J. Becker, C.-Y. Tsai, M. Boccard, Z. Holman, and Y.-H. Zhang, "1.7 eV MgCdTe solar cells for Si-based tandem applications," in 44th IEEE PVSC, Washington, DC (2017).
[15]M. Carmody, S. Mallick, J. Margetis, R. Kodama, T. Biegala, D. Xu, P. Bechmann, J. W. Garland, and S. Sivanathan, "Single-crystal II-VI and Si single-junction and tandem solar cells," Appl. Phys. Lett. **96**, 153502 (2010).
[16]T. Shimpi, J. Kephart, D. E. Swanson, A. Munshi, W. S. Sampath, A. Abbas, and J. M. Walls, "Effect of the cadmium chloride treatment on RF sputtered CdZnTe films for application in multijunction solar cells," J. Vac. Sci. Technol. A **34**, 051202 (2016).
[17]R. Dhere, K. Ramanathan, J. Scharf, H. Moutinho, B. To, A. Duda, and R. Noufi, "Investigation of CdMgTe Alloys for Tandem Solar Cell Applications," in *IEEE PVSC* (2006), Vol. 1, p. 546.
[18]C. Reich, D. E. Swanson, T. Shimpi, J. Drayton, A. Munshi, A. Abbas, and W. Sampath, "Passivation of CdMgTe absorber for application in a tandem cell," in *IEEE PVSC Portland* (2016), Vol. 1, p. 0487.
[19]B. E. McCandless, "Cadmium zinc telluride films for wide band gap solar cells," in *29th IEEE PVSC New Orleans* (2002), Vol. 1, p. 488.
[20]A. Abbas, D. Swanson, A. Munshi, K. L. Barth, W. S. Sampath, G. D. West, J. W. Bowers, P. M. Kaminski, and J. M. Walls, "The effect of a post-activation annealing treatment on thin film CdTe device performance," in 42nd IEEE PVSC (2015).
[21]S. H. Yoo, K. T. Butler, A. Soon, A. Abbas, J. M. Walls, and A. Walsh, "Identification of critical stacking faults in thin-film CdTe solar cells," Appl. Phys. Lett. **105**, 062104 (2014).
[22]E. S. Barnard, B. Ursprung, E. Colegrove, H. R. Moutinho, N. J. Borys, B. E. Hardin, C. H. Peters, W. K. Metzger, and J. P. Schuck, "3D lifetime tomography reveals how $CdCl_2$ improves recombination throughout CdTe solar cells," Adv. Mater. **29**, 1603801 (2017).
[23]C. Li, Y. Wu, J. Poplawsky, T. J. Pennycook, N. Paudel, W. Yin, S. J. Haigh, M. P. Oxley, A. R. Lupini, M. Al-Jassim, S. J. Pennycook, and Y. Yan, "Grain-boundary-enhanced carrier collection in CdTe solar cells," Phys. Rev. Lett. **112**, 156103 (2014).
[24]D. E. Swanson, J. M. Kephart, P. S. Kobyakov, K. Walters, K. C. Cameron, J. Drayton, J. R. Sites, K. L. Barth, and W. S. Sampath, "A single vacuum chamber with multiple close space sublimation sources to fabricate CdTe solar cells," J. Vac. Sci. Technol. A **34**, 021202 (2016).
[25]A. Moore, T. Song, and J. Sites, "Improved CdTe solar-cell performance with an evaporated Te layer before the back contact," MRS Adv. **2**, 3195–3201 (2017).
[26]J. M. Kephart, J. W. McCamy, Z. Ma, A. Ganjoo, F. M. Alamgir, and W. S. Sampath, "Band alignment of front contact layers for high-efficiency CdTe solar cells," Sol. Energy Mater. Sol. Cells **157**, 266 (2016).
[27]T. Song, A. Kanevce, and J. R. Sites, "Emitter/absorber interface of CdTe solar cells," J. Appl. Phys. **119**, 233104 (2016).
[28]D. E. Swanson, A. Abbas, A. H. Munshi, J. A. Drayton, J. M. Raguse, R. M. Geisthardt, J. R. Sites, and W. S. Sampath, "Incorporation of

$Cd_{1-x}Mg_xTe$ as an electron reflector for cadmium telluride photovoltaic cells," MRS Proc. **1771**, 133 (2015).
[29]J. Tauc, "Optical properties and electronic structure of amorphous Ge and Si," Mater. Res. Bull. **3**, 37 (1968).
[30]D. Kuciauskas, J. N. Duenow, A. Kanevce, J. V. Li, M. R. Young, P. Dippo, and D. H. Levi, "Optical-fiber-based, time-resolved photoluminescence spectrometer for thin-film absorber characterization and analysis of TRPL data for CdS/CdTe interface," in IEEE PVSC Austin (2012), Vol. 1, p. 160.
[31]H. R. Moutinho, R. G. Dhere, M. J. Ramero, C. S. Jiang, B. To, and M. M. Al-Jassim, "Recrystallization of PVD CdTe thin films induced by $CdCl_2$ treatment - A comparison between vapor and solution," in 33rd IEEE PVSC Conference, San Diego (2008).
[32]J. D. Major, R. E. Treharne, L. J. Phillips, and K. Durose, "A low-cost non-toxic post-growth activation step for CdTe solar cells," Nature **511**, 334 (2014).
[33]W. K. Metzger and M. Gloeckler, "The impact of charged grain boundaries on thin-film solar cells and characterization," J. Appl. Phys. **98**, 063701 (2005).
[34]B. Gaury and P. M. Haney, "Charged grain boundaries reduce the open-circuit voltage of polycrystalline solar cells - An analytical description," J. Appl. Phys. **120**, 234503 (2016).
[35]M. Gloeckler, J. R. Sites, and W. K. Metzger, "Grain-boundary recombination in Cu(In,Ga)Se_2 solar cells," J. Appl. Phys. **98**, 113704 (2005).
[36]W. K. Metzger, "The potential and device physics of interdigitated thin-film solar cells," J. Appl. Phys. **103**, 094515 (2008).